SciEn
Journal of Engineering Advancements Vol. 02(02) 2021, pp 95-103 https://doi.org/10.38032/jea.2021.02.005

Fabrication and Characterization of α-Fe_2O_3 Nanoparticles Dispersed Epoxy Nanocomposites

Muhammad Abdullah Al Mamun[1], Md. Abdus Sabur[1], Md. Abdul Gafur[2], Hrithita Aftab[1] and G. M. Shafiur Rahman[1]*

[1]Department of Materials Science and Engineering, University of Rajshahi, Rajshahi-6205, Bangladesh
[2]Institute of Pilot Plant and Process Development Centre, Bangladesh Council of Scientific and Industrial Research (BCSIR), Dhanmondi, Dhaka-1205, Bangladesh

Received: April 09, 2021, Revised: June 02, 2021, Accepted: June 06, 2021, Available Online: June 21, 2021

ABSTRACT

In this work, epoxy resin matrix based polymer nanocomposites were fabricated incorporating sol-gel synthesized hematite (α-Fe_2O_3) nanoparticles. The effect of nanoparticles on chemical, mechanical, electrical, optical and thermal properties in polymer matrix was evaluated. Different functional groups were present in α-Fe_2O_3 nanoparticles, neat epoxy and α-Fe_2O_3/epoxy nanocomposites that obtained from Fourier-Transform Infrared spectroscopy (FTIR). Vibrating Sample Magnetometer (VSM) analysis revealed that the α-Fe_2O_3 nanoparticles have superparamagnetic character. By incorporation of nanoparticles into the epoxy matrix decreased the tensile strength and elongation at break, and increased Young's modulus. In addition, the addition of nanoparticles into the epoxy matrix gradually reduced and increased of the flexural strength and hardness, respectively. The improvement in light absorbance of α-Fe_2O_3/epoxy nanocomposites was increased with increasing the α-Fe_2O_3 content. Conversely, the optical band gap was decreased with increasing nanoparticle addition.

Keywords: α-Fe_2O_3 Nanoparticles, Nanocomposites, Mechanical Properties, Epoxy Resin, Thermogravimetric Analysis (TGA).

1 Introduction

Organic-inorganic nanohybrid materials have been widely studied because of their unique properties resulting from the combination of both organic polymer and inorganic nanoparticles [1]-[8]. Also, there has been strong emphasis on the advancement of polymer nanohybrids, in which at least one of the dimensions of the filler has nanometer scale. Researchers have long known that decreasing filler dimension increases the specific surface area of the filler, which in turn may effectively improve the transfer of the load between the polymer matrix and fillers. These nanohybrid materials may exhibit significant enhancements in thermal, mechanical, and electrical properties that are difficult to achieve using conventional fillers with micro scale dimensions, such as carbon, glass, or aramid fibres. In order to reduce the gap between the performances of today's engineering polymers and the ever-increasing demand of engineering applications, new nanohybrids are needed with optimum nanofillers dispersion, improved load transfer-ability from polymer to filler particles, and enhanced thermal properties. Generally, the reinforcement of nano-particles into the polymer matrix enhances the mechanical, dimensional, and thermal stability of the host polymer matrix.

Hematite (α-Fe_2O_3) nanoparticle is an inorganic nanofiller, exhibits some excellent properties like- low cost, environmentally friendly, low toxicity, corrosion and chemically resistance, biocompatibility, and good substrate adherence [7],[8]. Because of these excellent properties, α-Fe_2O_3 nanoparticles are used in water treatment [9], contrast reagents/drug delivery [10], sensor technology [11],[12], optical coatings, magnetic storage [13], field-effect transistors [14], catalysts [15], pigments [16], etc. α-Fe_2O_3 nanoparticles can be synthesized by several methods, for instance, chemical vapour deposition, hydrothermal synthesis [17], sonochemical technique, chemical precipitation [18], sol-gel technique [19], microemulsion technique [20], hydrolysis [21], ball milling [22], laser ablation, sputtering, and spray pyrolysis [23]. In the past decades until now, there have been numerous investigations of different magnetic nanoparticle-based polymer nanocomposites [24]-[30]. A few examples are mentioned here. In 2008, Dusko Dudic et al. studied the electrical properties of a composite comprising epoxy resin and α-Fe_2O_3 nanorods [24]. In 2017, Prasanna B P et al. synthesized polyaniline/α-Fe_2O_3 nanocomposite electrode material for super-capacitor applications [25]. In 2016, Ali Mirzaei et al. synthesized and characterized mesoporous α-Fe_2O_3 nanoparticles to investigate the electrical properties of fabricated thick films [26].

On the other hand, epoxy resin is a thermosetting polymer with some excellent properties e.g. light weight, chemically resistance, oil and fuel resistance, electrical insulator, etc. Because of these features epoxy can be used in LEDs, printed circuit boards, inductors, marine applications, coatings, structural adhesives, electrical insulators, and other electrical, electronics, and industrial applications [27]. In 2011, Richard Voo et al. studied different properties of epoxy nanocomposite films [28]. In 2016, A. Kanapitsas et al. studied the dielectric, magnetic, and hydration behaviour of barium ferrite/epoxy nanocomposites [29]. In 2016, Masoomeh Gazderazi et al. studied the mechanical and thermal properties of hybridizing MWCNT with nano metal oxides and TiO_2 in epoxy composite [30]. The incorporation of nanofillers into the polymer matrix not

*Corresponding Author Email Address: mamun_mse@ru.ac.bd Published by: SciEn Publishing Group

only improves the mechanical properties, besides it also helps to extend the application of fabricated nanocomposite [31],[34].

According to previous reports, most work in this field has been done to fabricate α-Fe_2O_3 nanocomposites or Epoxy composites individually. Also, less importance was given to evaluate the mechanical, thermal, and optical properties of α-Fe_2O_3/epoxy nanocomposites. Therefore, the main objective of this work is to synthesized α-Fe_2O_3 nanoparticles which are further dispersed into the epoxy matrix to improve the mechanical and thermal properties as well as optical and electrical properties of α-Fe_2O_3/epoxy nanocomposites.

In the present study, nanocomposites containing epoxy and α-Fe_2O_3 nanoparticles with various compositions were fabricated by solution casting method on flat glass mold. The samples were characterized by various experimental techniques, and the influence of α-Fe_2O_3 nanoparticles on the mechanical, thermal, optical, and electrical properties of α-Fe_2O_3/epoxy nanocomposites was investigated.

2 Experimental Details

2.1 Materials

All the chemical reagents were of analytical grade and used without further purification. Anhydrous ferric nitrate ($Fe(NO_3)_3$), Anhydrous citric acid ($C_6H_8O_7$) were purchased from Merck (India) with a purity ≥98 %, whereas epoxy resin and diethylene triamine (DETA) hardener were purchased from Sigma-Aldrich (India).

2.2 Synthesis of α-Fe_2O_3 Nanoparticles

Hematite (α-Fe_2O_3) nanoparticles were chemically synthesized by sol-gel process, where 200 mL (0.1M) of anhydrous ferric nitrate, $Fe(NO_3)_3$ used as a precursor solution which gelated by using 800 mL (0.1M) of anhydrous citric acid, $C_6H_8O_7$ solution as ligand molecules, and singly distilled water as the solvent. Ferric nitrate solution drop-wise added to the citric acid solution with maintaining vigorous stirring by magnetic stirrer. The mixture was heated to 70 °C and continuous stirring was maintained until the gel formation. The produced gel was then dried by evaporation. After that, the dried gel was annealed at 250 ^{0}C for 1.5 hours. Finally, the powder was grinding by mortar and pestle, typically yielding 0.85gm of α-Fe_2O_3 nanoparticles.

2.3 Fabrication of α-Fe_2O_3/Epoxy Nanocomposites

In order to fabricate the nanocomposites, a certain amount of α-Fe_2O_3 nanoparticles was added into epoxy resin and mixed carefully for 15 minutes to get a uniform dispersion of the nanoparticles within the resin. After that, the curing agent diethylene triamine (DETA) was added with continuous stirring (epoxy-curing agent ratio was 10:1 by weight). Finally, the above mixture was cast into a flat glass mold and out-gassed overnight. The produced composite sheets had an approximate thickness of 2 mm. Due to their high aspect ratio and large surface area, the contents of the α-Fe_2O_3 nanoparticles in the composite were chosen to be 0.5, 1.0, 2.5, and 5.0 wt% respectively.

2.4 Characterization Techniques

2.4.1 X-Ray Diffraction (XRD)

The XRD patterns of α-Fe_2O_3 nanoparticles were obtained using a BRUKAR ADVANCE D8 Diffractometer. The diffraction patterns were measured at room temperature using Cu Kα radiation (λ = 1.5406 Å) where Bragg's angles varying from 10º to 70º.

2.4.2 Scanning Electron Microscopy (SEM)

The morphologies and microstructures of α-Fe_2O_3 nanoparticles were observed using JEOLUSER 7610F Scanning Electron Microscope, which operated at 5 kV.

2.4.3 Fourier-Transform Infrared Spectroscopy (FTIR)

The presence of different functional groups in α-Fe_2O_3 nanoparticles, neat epoxy and α-Fe_2O_3/epoxy nanocomposites were observed using PERKIN-ELMER FRONTIER FTIR/MIR Spectrometer. The FTIR spectra were recorded in the 450-4000 cm^{-1} region.

2.4.4 Vibrating Sample Magnetometer (VSM)

The magnetization-magnetic field hysteresis loops of α-Fe_2O_3 nanoparticles were measured by using ***MICROSENSE EV9 Vibrating Sample Magnetometer*** at room temperature.

2.4.5 Tension and Flexural testing

The tensile tests of neat epoxy and α-Fe_2O_3/epoxy nanocomposites were conducted according to ASTM D882 (2012) using a Universal Testing Machine (Hounsfield UTM 10KN, UK). The clamping length for each specimen on each jaw was 15 mm, and no extensometer was used for the tensile tests. The tests were performed at a crosshead speed of 5 mm/min. Each value reported is the average of five sample tests. The flexural strength of neat epoxy and α-Fe2O3/epoxy nanocomposites were measured using HOUNSFIELD H10KN UTM according to the standard method used for flexural properties (ASTM D790-98 2003). The speed for the flexural test was set at 5 mm/min. In addition, each value reported is the average of five sample tests.

2.4.6 Hardness Testing

The hardness of neat epoxy and α-Fe_2O_3/epoxy nanocomposites were measured using SHIMADZU HMV-2 VICKER'S Micro-Hardness Tester. The specimen was placed on a hard, horizontal glass surface. The diamond indenter was held vertically and the scale was measured with 10 seconds, after the pressure was in firm contact with the specimen. Each sample was investigated five times at a certain load with 10 s indentation time.

2.4.7 Thermogravimetric Analysis (TGA)

The TGA curves of α-Fe_2O_3 nanoparticles, neat epoxy andα-Fe_2O_3/epoxy nanocomposites were determined using EXSTAR 6000, TG/DTA 6300 Thermal Analyzer. The rate of heating was 20 ºC/min and the mass of the specimen was 2-3 mg. The measurements were carried out in nitrogen atmosphere.

2.4.8 UV-Vis Spectroscopy

The optical absorption of neat epoxy and α-Fe_2O_3/epoxy nanocomposites were recorded at room temperature using SHIMADZU UV-1601 Spectrophotometer in the range of 190-1100 nm.

2.4.9 DC Resistivity

The DC resistivity of neat epoxy and α-Fe_2O_3/epoxy nanocomposites were determined using KEITHLEY 6517B Electrometer at room temperature where the applied voltages were 10, 20, 30, 40, 50 volts, respectively for every sample.

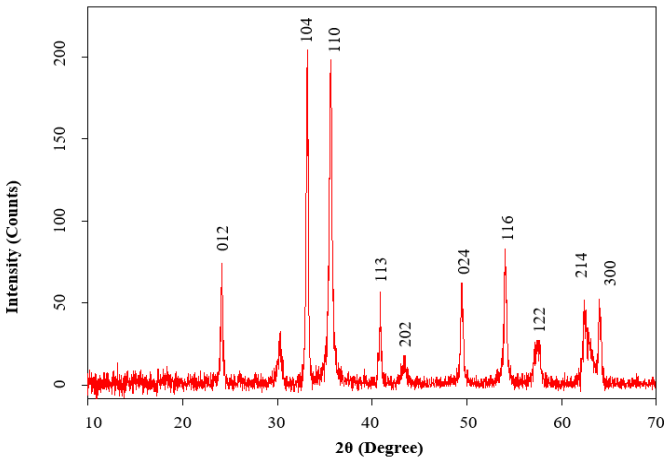

Fig. 1 XRD patterns of α-Fe_2O_3 nanoparticles

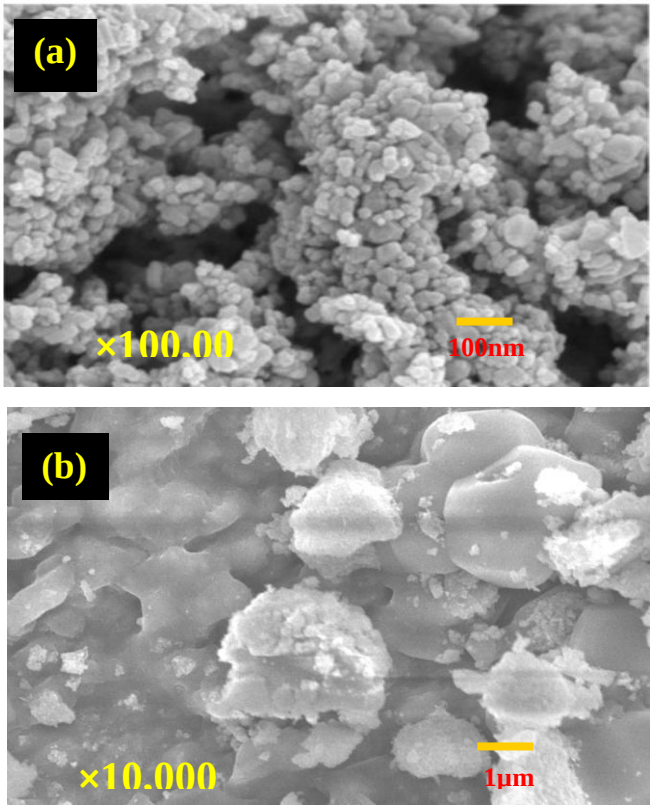

Fig. 2 SEM images of (a) α-Fe_2O_3 nanoparticles and (b) α-Fe_2O_3/Epoxy nanocomposite.

3 Results and Discussion

3.1 XRD Analysis

The XRD patterns of α-Fe_2O_3 nanoparticles produced by the sol-gel process were illustrated in Fig. 1. The XRD peaks were recorded with the 2θ value varying from 10° to 70° with Cu Kα radiation (λ=1.5406Å). The XRD patterns of α-Fe_2O_3 were indexed as pure hexagonal structures. The peaks were appeared at 2θ values of 24.118°, 33.2432°, 35.6757°, 40.89°, 43.41°, 49.47°, 54.069°, 57.46°, 62.327°, and 64.0° and represented by the (012), (104), (110), (113), (202), (024), (116), (122), (214) and (300) crystalline structures correspond to pure α-Fe_2O_3 nanoparticles. The diffraction peaks matched with standard JCPDS card no. 87-1164 [35], indicating that the α-Fe_2O_3 nanoparticles are crystalline structures. The average crystallite sizes were calculated by using the Debye-Scherer equation:

$$D = \frac{K\lambda}{\beta cos\theta}$$

where K is the shape factor (the typical value is 0.94), λ is the wavelength of the incident beam, β is the broadening of the diffraction line measured in radians at half of its maximum intensity (FWHM) and θ is the Bragg's angle and D is the diameter of the crystallite size [36]. The average crystallite sizes of α-Fe_2O_3 from the XRD data were found to be around 32 nm. No other peaks were observed in the calcined compound, which indicates the formation of a pure hexagonal structure of α-Fe_2O_3 nanoparticles.

3.2 SEM Analysis

The SEM images of α-Fe_2O_3 nanoparticles and α-Fe_2O_3/epoxy nanocomposites are illustrated in Fig. 2(a) and (b), with ×100,000 and ×10,000 magnification, respectively. Fig. 2(a) shows α-Fe_2O_3 nanoparticles are well defined and oriented spindle-like with small spherical shaped particles. The average crystallite size of α-Fe_2O_3 which was calculated from the SEM image was found to be around 29 nm. From Fig. 2(a), it is clear that α-Fe_2O_3 nanoparticles are mainly present as granules with small spherical-shaped particles and are well crystalline.

Due to the very tiny particle size, the number of existing atoms/molecules on the surface was increased excessively. Therefore, the agglomeration of nanoparticles was seen due to the presence of inter-particle forces such as electrostatic forces, van der waals forces.

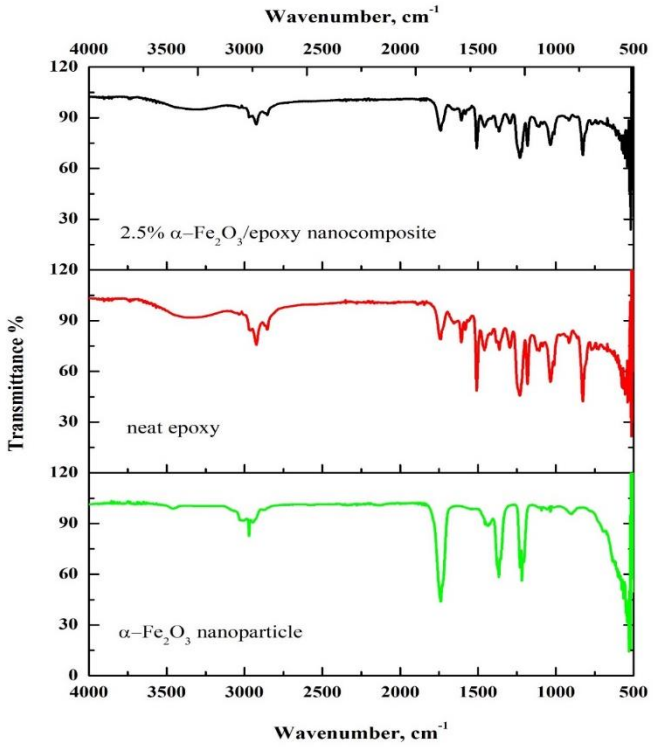

Fig. 3 FTIR spectrum of α-Fe_2O_3 nanoparticles, neat epoxy and 2.5% α-Fe_2O_3/epoxy nanocomposite

During the synthesis and process of nanoparticles this agglomeration commonly occurs [34]. From Fig. 2(b), it is seen that the α-Fe_2O_3 nanoparticles are more or less uniformly confined in the epoxy matrix. The inclusion of nano-sized particles impart new properties compared to polymer matrix

itself. The mechanical properties of composites either positively or negatively influences by the size of nanoparticles [35].

In composite systems, it is found that the mechanical properties such as strength, rigidity and yield strength varies with the size of incorporated particles [35].

3.3 FTIR Analysis

Fig. 3 shows the FTIR spectra of α-Fe_2O_3 nanoparticles, neat epoxy, and 2.5% α-Fe_2O_3/epoxy nanocomposite. For α-Fe_2O_3 nanoparticles, the band at 3466 cm^{-1} is assigned to the stretching vibration of water, indicating the existence of a little water absorbed on the sample. The high-frequency band at 544 cm^{-1} refers to Fe-O deformation in the octahedral and tetrahedral sites which gives evidence for the formation of α-Fe_2O_3.

There is no peak at 2900 cm^{-1} indicating the C-H stretching band, which means all organic compounds are removed from the samples after calcination at 250 °C. For neat epoxy, the O-H, C-H, C=O, C=C, C=N, and C-O stretching vibration peaks are located at 3370, 2926, 1748, 1510, 1238, and 1037 cm^{-1}, respectively. The C-H bending vibration peak is located at 1366 cm^{-1}. For 2.5% α-Fe_2O_3/epoxy nanocomposite, the O-H, C-H, C=O, C=C, C-N, and C-O stretching vibration peaks are located at 3328, 2933, 1749, 1509, 1234, and 1039 cm^{-1}, respectively. The C-H bending vibration peak is located at 1371 cm^{-1}.

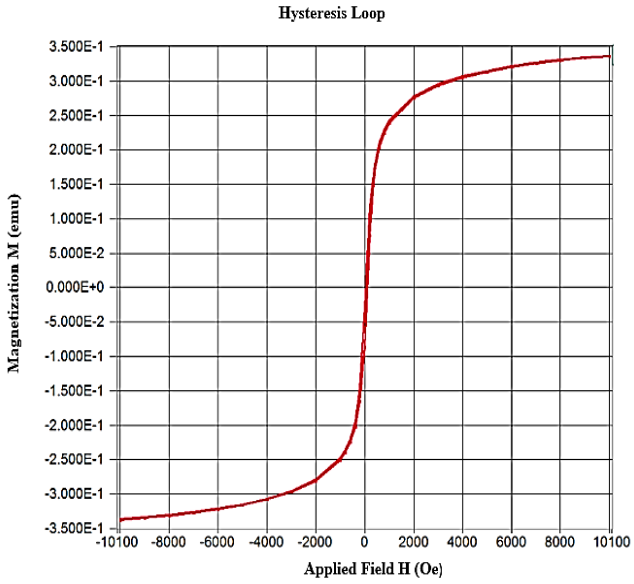

Fig. 4 Magnetization-magnetic field hysteresis curve of α-Fe_2O_3 nanoparticles.

3.4 VSM Analysis

The magnetic properties of α-Fe_2O_3 nanoparticles were measured by a vibrating sample magnetometer. Fig. 4 illustrates the magnetic hysteresis curve of α-Fe_2O_3 nanoparticles recorded at room temperature. It exhibits superparamagnetic behavior due to nanoscale particle size. The saturation magnetization (M_s), coercivity (H_c), and remnant magnetization (M_r) of α-Fe_2O_3 nanoparticles were 337.137×10^{-3} emu, 33.312 Oe, and 28.90×10^{-3} emu, respectively. It should be mentioned that the magnetic properties of the materials depend on the particle's size, shape, magnetization direction, crystallinity, etc.

3.5 Tensile Properties Analysis

Fig. 5 represents the stress-strain curves of neat epoxy, 0.5, 1.0, 2.5, and 5.0 wt% of α-Fe_2O_3/epoxy nanocomposites. Epoxy is a brittle material because it fails in tension at relatively low values of strain. In Fig. 5, the stress-strain curves which remain straight initially represent the elastic region, where the stress and strain are directly proportional. The elastic modulus of the material was measured from the slope of 0.1 to 0.25% tensile strain. Fig. 6 demonstrates the measured tensile properties of α-Fe_2O_3/epoxy nanocomposites. It can be seen that the presence of α-Fe_2O_3 nanoparticles enhanced the tensile stress-strain behavior of the epoxy polymer. Nanocomposites show higher tensile modulus. The increase in modulus is expected because the modulus of α-Fe_2O_3 nanoparticles is about 359 GPa.

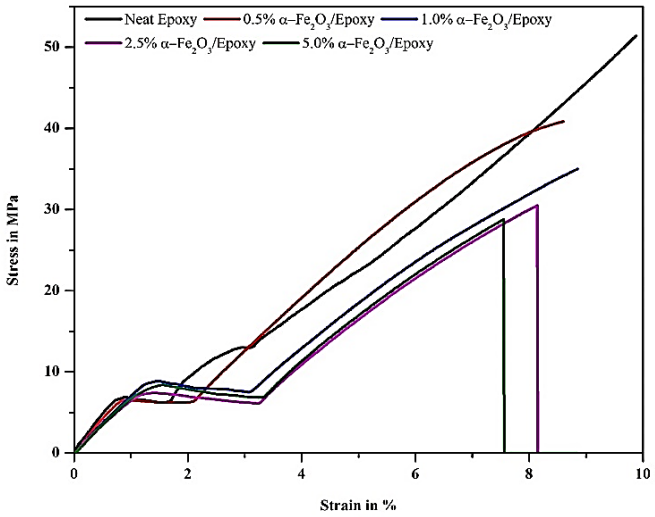

Fig. 5 Stress-strain curve of α-Fe_2O_3/epoxy nanocomposites.

The incorporation of α-Fe_2O_3 nanoparticles into epoxy matrix decreased the tensile strength of the nanocomposites because epoxy resin and α-Fe_2O_3 nanoparticles both are brittle materials. Sometimes, agglomeration of nanoparticles inside the polymer matrices becomes responsible for decreasing the tensile strength. This implies that the interfacial bonding between matrix and particle is not strong enough to bear large mechanical stress, as because of inhomogeneous dispersion of nanoparticles. The presence of highly stiff α-Fe2O3 nanoparticles in the polymer matrix is responsible for lowering the elastic modulus and elongation of the polymer [37].

Table 1 Flexural properties of neat epoxy and α-Fe_2O_3/epoxy nanocomposites

Materials	Flexural Strength (MPa)	Strain at Break (%)	Energy (Joule)
Neat epoxy	84.50	1.735	0.0601
0.5% α-Fe_2O_3 /epoxy	76.50	2.127	0.0633
1.0% α-Fe_2O_3 /epoxy	64.50	2.279	0.0338
2.5% α-Fe_2O_3 /epoxy	59.30	1.563	0.0236
5.0% α-Fe_2O_3 /epoxy	53.00	1.850	0.0293

3.6 Flexural Properties Analysis

The three-point flexural test was carried out to determine the flexural properties of α-Fe_2O_3/epoxy nanocomposites, whose force-extension curves are shown in Fig. 7. The neat epoxy, 0.5, 1.0, 2.5, and 5.0 wt% of α-Fe_2O_3/epoxy nanocomposites exhibit

84.5, 76.5, 64.5, 59.3 and 53.0 MPa flexural strength with 1.735, 2.127, 2.279, 1.563 and 1.850% strain at break, respectively which are illustrated in Table 1. From Table 1 we can see that, the addition of α-Fe_2O_3 nanoparticles into the epoxy matrix gradually reduced the flexural strength of the nanocomposites, the reason is due to the compressive characteristics of epoxy resin and α-Fe_2O_3 nanoparticles. The addition of filler is not much effective in flexural characteristics of the matrix but it may increase in the case of laminates with filler matrix [38].

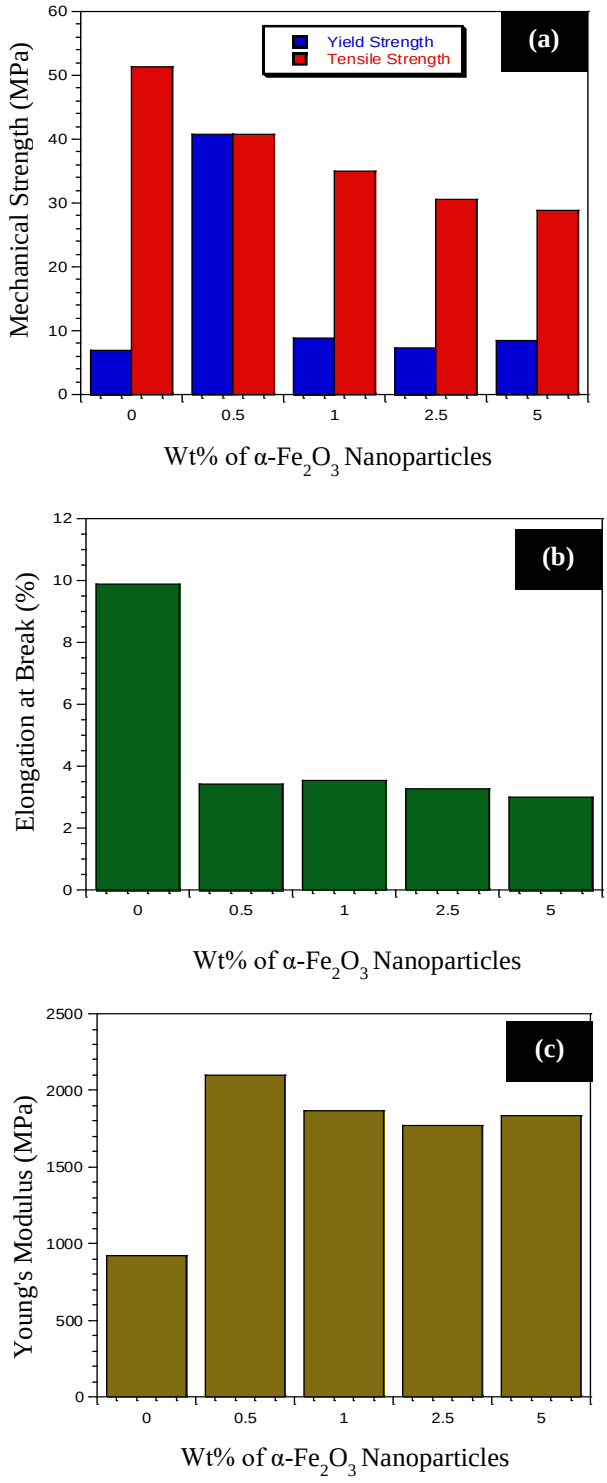

Fig. 6 Effect of different nanoparticles addition on (a) Mechanical Strength (b) Elongation, and (c) Young's modulus in epoxy polymer matrix.

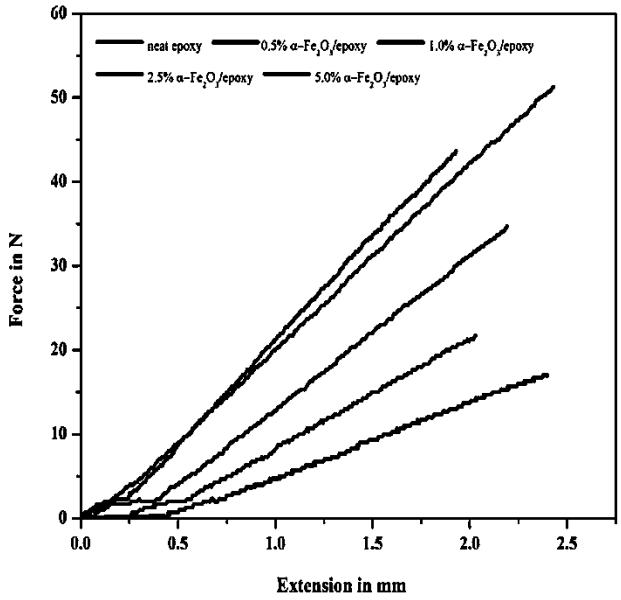

Fig. 7 Force-extension curves of α-Fe_2O_3/epoxy nanocomposites

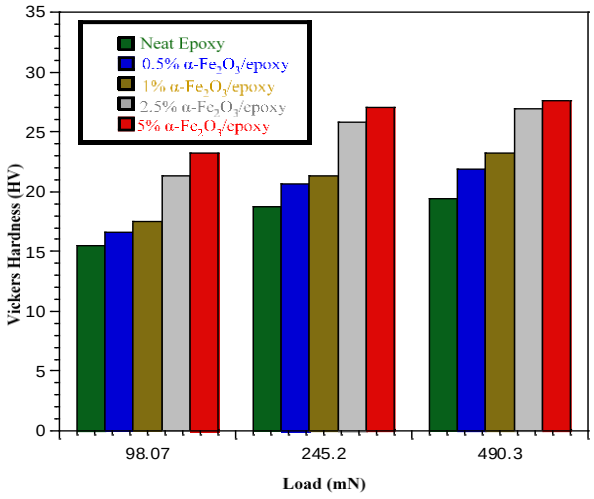

Fig. 8 Vickers hardness number of neat epoxy and α-Fe_2O_3/epoxy nanocomposites.

3.7 Hardness Analysis

Hardness is the ability of a material to resist plastic deformation, usually by penetration. However, it may also refer to the resistance to bending, scratching, abrasion or cutting. The hardness of neat epoxy, 0.5, 1.0, 2.5, and 5.0 wt% of α-Fe_2O_3/epoxy nanocomposites was measured by Vickers's micro-hardness tester. These tests were performed at three different loads 98.07, 245.2, and 490.3 mN, respectively, and the results are shown in Fig. 8. The measured values of hardness increased considerably for α-Fe_2O_3/epoxy nanocomposites due to the addition of stiff nanoparticles in the polymer matrix. The successful interaction between nanoparticles and polymer matrix helped to transfer the applied load from matrix to nanoparticles. Thus, the applied load became suppressed by the stiff nanoparticles and the hardness value increased in the composites compared to that of the neat epoxy matrix. In addition incorporation of α-Fe_2O_3 nanoparticles into epoxy resist the movement of dislocation within the structure of the epoxy matrix, increases hardness.

3.8 TG Analysis

Fig. 9 shows the TG curve of α-Fe_2O_3 nanoparticles, neat epoxy, and 5.0% α-Fe_2O_3/epoxy nanocomposite, respectively. The decomposition process consists of three regions. They were 20-300 ºC, 300-500 ºC, and 500-600 ºC, respectively. The first weight loss indicates the evaporation of absorbed water due to the initial breakdown of the complex and spontaneous combustion. H_2O and CO_2 provide an oxidizing environment for the combustion of the organic components [39], citrate ions in the gel cause spontaneous combustion. The second weight-loss indicates the dehydration of the O-H group in the α-Fe_2O_3 structure and epoxy that lead to two degradation systems involving both inter and intra-molecular transfer reaction, the oxidation of complexes, and formation of semi-organic carbon metal/metal oxide [40]-[42].

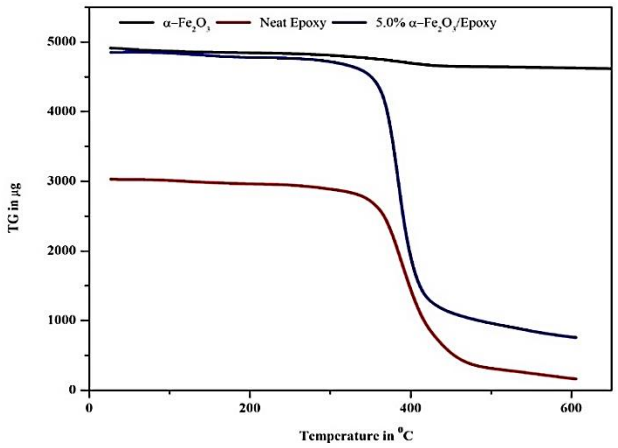

Fig. 9 TGA curve of α-Fe_2O_3 nanoparticles, neat epoxy and 5.0% α-Fe_2O_3/epoxy nanocomposite

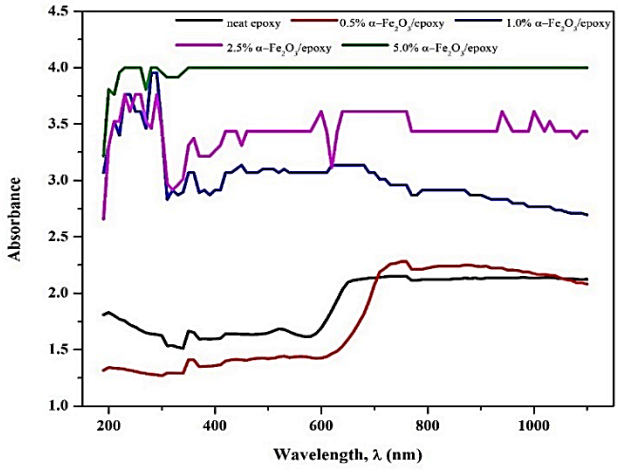

Fig. 10 Absorbance vs wavelength curve of α-Fe_2O_3/epoxy nanocomposites

The third weight loss indicates the formation of the corresponding metal oxide phase. Above 600 ^{0}C there is no weight loss i.e. the TGA curve is steady, exhibiting the absolute volatility of water, organic compounds, citrates in the composites, the completion of crystallization route, and the immediate formation of pure materials.

3.9 UV-Vis Spectroscopy Analysis

UV-Vis spectroscopy is used to determine the optical band gap energy of crystalline and amorphous materials. In this method, electron excitation from the valance band to the conduction band, is used to verify the character and value of the optical band gap. UV-visible spectra of fabricated specimens were measured in the 190-1100 nm range, (Fig. 10). The spectrum of neat epoxy shows a single absorption peak at 526 nm, which represents the polaron/bipolaron transition. On the other hand, spectra of α-Fe_2O_3/epoxy nanocomposites show several peaks within the entire range in shells increase the absorption cross-section of the nanocomposite and thus enhance plasma-exciton interactions [43]-[45]. The optical band gap is determined using the following relationship [46]:

$$\alpha h\upsilon^{\frac{1}{n}} = A(h\upsilon - E_g) \quad (1)$$

For direct band gap materials this equation becomes-

$$\alpha h\upsilon = A(h\upsilon - E_g)^2 \quad (2)$$

where α is the absorption coefficient, A is a constant, E_g is the optical band gap of the material and the exponent n depends on the nature of electronic transition, it is equal to 1/2 for direct allowed, 3/2 for direct forbidden transitions, and 2 for indirect allowed transition. An extrapolation of the linear region of a plot of the graph of $(\alpha h\upsilon)^2$ on the y-axis versus photon energy (hυ) on the x-axis, gives the value of the optical band gap, E_g [47]. The optical band gap is calculated and shown in Fig. 11. From Fig. 10, we can see that, the absorbance of α-Fe_2O_3/epoxy nanocomposites increased with increasing the α-Fe_2O_3 content. The increased light absorption phenomena can be attributed to the well dispersion and successful interaction of nanoparticles inside the polymer matrix.

Conversely, from Fig. 11, we can see that, the optical band gap of neat epoxy, 0.5, 1.0, 2.5, and 5.0 wt% of α- Fe_2O_3/epoxy nanocomposites were 3.2, 2.8, 2.4, 1.8, and 1.4 eV, respectively. This decrease of E_g can be attributed to the formation of complex due to interaction between nanoparticles and polymer matrix. In addition, the increase of density of defects i.e. particle clusters leads to the expansion of valance band inside the forbidden gap of polymeric system. Therefore, band tailing occurred and as a consequence shrinkage of Eg was happened [48].

3.10 DC Resistivity Analysis

Fig. 12 shows the I-V curves of neat epoxy, 0.5, 1.0, 2.5 and 5.0 wt% of α-Fe_2O_3/epoxy nanocomposites, where all the tests were performed at room temperature. This figure indicates that 5.0 % α-Fe_2O_3 nanoparticles containing epoxy nanocomposite have the higher value of dc current, I (about 27.342 nA) at 50 volts, whereas neat epoxy shows the minimum value of dc current, I (about 18.741 pA) at 10 volts. On the other hand, Fig. 13 shows the variation of measured dc resistivity (ρ) of neat epoxy, 0.5, 1.0, 2.5 and 5.0 wt% of α-Fe_2O_3/epoxy nanocomposites. This figure illustrates that neat epoxy exhibits the highest value of dc resistivity, ρ (about 3.017 TΩmm) because epoxy is an excellent electrically insulating material, whereas 2.5% α-Fe_2O_3/epoxy nanocomposite exhibits the lowest value of dc resistivity, ρ (about 0.923 TΩmm).

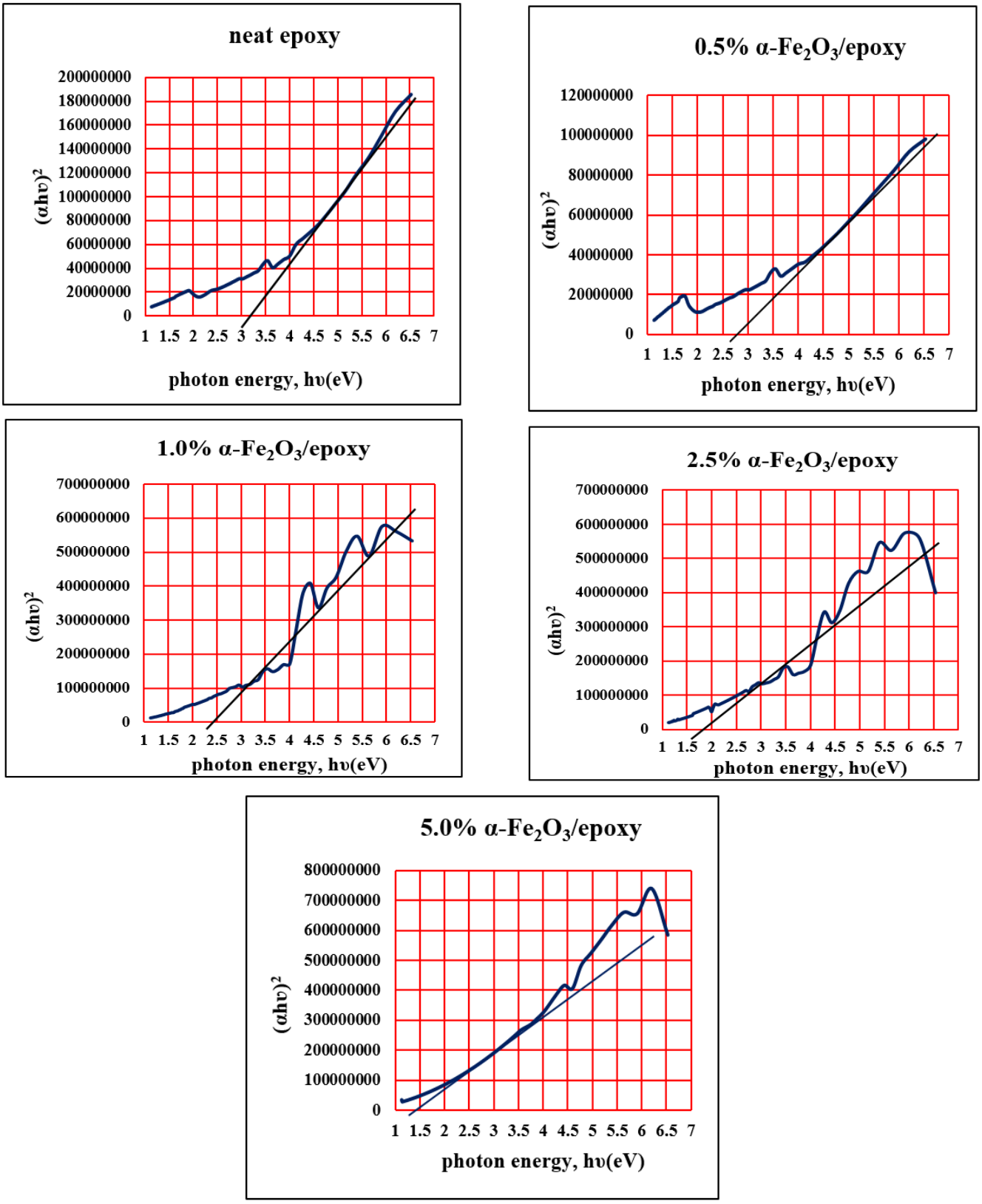

Fig. 11 Optical band gap of α-Fe_2O_3/epoxy nanocomposites

By increasing the α-Fe_2O_3 content into epoxy, the dc resistivity of the nanocomposite sheets decreased gradually due to the formation of polarons in the both epoxy and α-Fe_2O_3 molecules after applying voltage [49]. By increasing α-Fe_2O_3 content, the dc resistivity changes slightly, which attributed to saturation of charge carriers.

However, 1.0% α-Fe_2O_3/epoxy nanocomposite exhibited a little inconsistency of dc resistivity may be due to the non-

uniform dispersion and agglomeration of α-Fe_2O_3 nanoparticles into the epoxy matrix. Moreover, this happened due to the dispersion of higher amount of nanoparticles than the critical volume fraction in the polymer matrix.

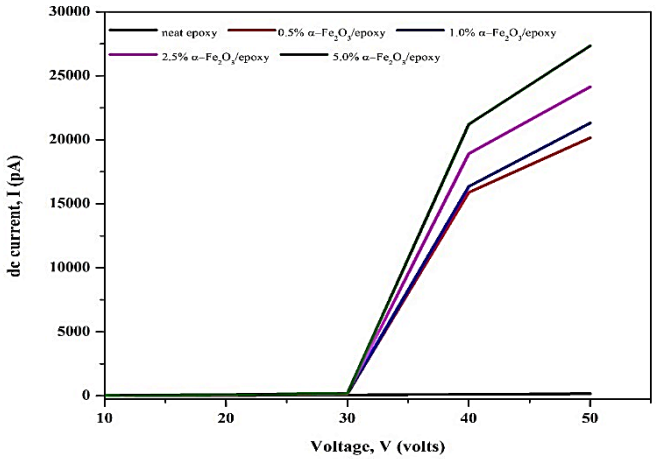

Fig. 12 I-V curves of α-Fe_2O_3/epoxy nanocomposites

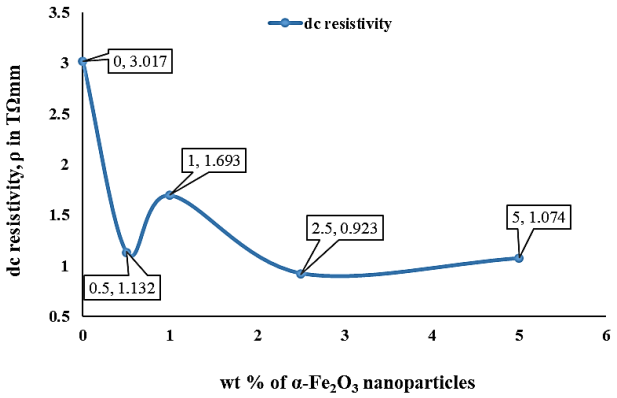

Fig. 13 Effect of α-Fe_2O_3 nanoparticles on the dc resistivity of α-Fe_2O_3/epoxy nanocomposites

4 Conclusions

In this study, we synthesized α-Fe_2O_3 nanoparticles by sol-gel process which further dispersed into the epoxy matrix to fabricate nanocomposites. The chemical, mechanical, electrical, optical and thermal properties of the fabricated polymer nanocomposites were evaluated. The XRD and SEM confirmed the formation of nanoparticles. FTIR analysis ensured the presence of different functional groups into the nanomaterials. Using VSM measurement, the saturation magnetization (M_s), coercivity (H_c) and remnant magnetization (M_r) of α-Fe_2O_3 nanoparticles were found to be 337.137×10^{-3} emu, 33.312 Oe and 28.90×10^{-3} emu, respectively. Incorporation of α-Fe_2O_3 nanoparticles into epoxy matrix gradually decreased tensile strength, elongation, flexural strength, optical band gap energy and dc resistivity of α-Fe_2O_3/epoxy nanocomposites, however, increased the young modulus, surface hardness and thermal stability of α-Fe_2O_3/epoxy nanocomposites. The fabricated nanocomposites can be used to produce various products in medical, construction, automotive, etc. sectors with better properties based on the obtained results.

References

[1] Huynh, W.U., Dittmer, J.J. and Alivisatos, A.P., 2002. Hybrid nanorod-polymer solar cells. Science, 295(5564), pp.2425-2427.

[2] Lu, Y., Yang, Y., Sellinger, A., Lu, M., Huang, J., Fan, H., Haddad, R., Lopez, G., Burns, A.R., Sasaki, D.Y. and Shelnutt, J., 2001. Self-assembly of mesoscopically ordered chromatic polydiacetylene/silica nanocomposites. Nature, 410(6831), pp.913-917.

[3] Wang, G.F., Tao, X.M. and Wang, R.X., 2008. Flexible organic light-emitting diodes with a polymeric nanocomposite anode. Nanotechnology, 19(14), p.145201.

[4] McDonald, S.A., Konstantatos, G., Zhang, S., Cyr, P.W., Klem, E.J., Levina, L. and Sargent, E.H., 2005. Solution-processed PbS quantum dot infrared photodetectors and photovoltaics. Nature Materials, 4(2), pp.138-142.

[5] Podsiadlo, P., Kaushik, A.K., Arruda, E.M., Waas, A.M., Shim, B.S., Xu, J., Nandivada, H., Pumplin, B.G., Lahann, J., Ramamoorthy, A. and Kotov, N.A., 2007. Ultrastrong and stiff layered polymer nanocomposites. Science, 318(5847), pp.80-83.

[6] Wang, L., Yoon, M.H., Lu, G., Yang, Y., Facchetti, A. and Marks, T.J., 2006. High-performance transparent inorganic–organic hybrid thin-film n-type transistors. Nature Materials, 5(11), pp.893-900.

[7] Shan, H., Liu, C., Liu, L., Li, S., Wang, L., Zhang, X., Bo, X. and Chi, X., 2013. Highly sensitive acetone sensors based on La-doped α-Fe2O3 nanotubes. Sensors and Actuators B: Chemical, 184, pp.243-247.

[8] Sun, Y., Guo, G., Yang, B., Cai, W., Tian, Y., He, M. and Liu, Y., 2011. One-step solution synthesis of Fe2O3 nanoparticles at low temperature. Physica B: Condensed Matter, 406(4), pp.1013-1016.

[9] Fang, X.L., Chen, C., Jin, M.S., Kuang, Q., Xie, Z.X., Xie, S.Y., Huang, R.B. and Zheng, L.S., 2009. Single-crystal-like hematite colloidal nanocrystal clusters: synthesis and applications in gas sensors, photocatalysis and water treatment. Journal of Materials Chemistry, 19(34), pp.6154-6160.

[10] Gupta, A.K. and Gupta, M., 2005. Synthesis and surface engineering of iron oxide nanoparticles for biomedical applications. Biomaterials, 26(18), pp.3995-4021.

[11] Mirzaei, A., Janghorban, K., Hashemi, B., Bonavita, A., Bonyani, M., Leonardi, S.G. and Neri, G., 2015. Synthesis, characterization and gas sensing properties of Ag@ α-Fe2O3 core–shell nanocomposites. Nanomaterials, 5(2), pp.737-749..

[12] Neri, G., Bonavita, A., Galvagno, S., Siciliano, P. and Capone, S., 2002. CO and NO2 sensing properties of doped-Fe2O3 thin films prepared by LPD. Sensors and Actuators B: Chemical, 82(1), pp.40-47.

[13] Mitra, S., Das, S., Mandal, K. and Chaudhuri, S., 2007. Synthesis of a α-Fe2O3 nanocrystal in its different morphological attributes: growth mechanism, optical and magnetic properties. Nanotechnology, 18(27), p.275608.

[14] Fan, Z., Wen, X., Yang, S. and Lu, J.G., 2005. Controlled p-and n-type doping of Fe 2 O 3 nanobelt field effect transistors. Applied Physics Letters, 87(1), p.013113.

[15] Wagloehner, S., Reichert, D., Leon-Sorzano, D., Balle, P., Geiger, B. and Kureti, S., 2008. Kinetic modeling of the oxidation of CO on Fe2O3 catalyst in excess of O2. Journal of Catalysis, 260(2), pp.305-314..

[16] Pailhé, N., Wattiaux, A., Gaudon, M. and Demourgues, A., 2008. Impact of structural features on pigment properties of α-Fe2O3 haematite. Journal of Solid State Chemistry, 181(10), pp.2697-2704.

[17] Hu, C., Gao, Z. and Yang, X., 2007. Facile synthesis of single crystalline α-Fe2O3 ellipsoidal nanoparticles and its catalytic performance for removal of carbon monoxide. Materials Chemistry and Physics, 104(2-3), pp.429-433.

[18] Eivari, H.A. and Rahdar, A., 2013. Some properties of iron oxide nanoparticles synthesized in different conditions. World Appl. Program, 3(2), pp.52-55.

[19] Bandgar, D.K., Navale, S.T., Khuspe, G.D., Pawar, S.A., Mulik, R.N. and Patil, V.B., 2014. Novel route for fabrication of nanostructured α-Fe2O3 gas sensor. Materials Science in Semiconductor Processing, 17, pp.67-73.

[20] Ramesh, R., Ashok, K., Bhalero, G.M., Ponnusamy, S. and Muthamizhchelvan, C., 2010. Synthesis and properties of α-Fe2O3 nanorods. Crystal Research and Technology, 45(9), pp.965-968.

[21] Yan, H., Su, X., Yang, C., Wang, J. and Niu, C., 2014. Improved photocatalytic and gas sensing properties of α-Fe2O3 nanoparticles derived from β-FeOOH nanospindles. Ceramics International, 40(1), pp.1729-1733.

[22] Mahmoud, M.H., Hamdeh, H.H., Ho, J.C., O'shea, M.J. and Walker, J.C., 2000. Mössbauer studies of manganese ferrite fine particles processed by ball-milling. Journal of Magnetism and Magnetic Materials, 220(2-3), pp.139-146.

[23] Shinde, S.S., Moholkar, A.V., Kim, J.H. and Rajpure, K.Y., 2011. Structural, morphological, luminescent and electronic properties of sprayed aluminium incorporated iron oxide thin films. Surface and Coatings Technology, 205(12), pp.3567-3577.

[24] Dudić, D., Marinović-Cincović, M., Nedeljković, J.M. and Djoković, V., 2008. Electrical properties of a composite comprising epoxy resin and α-hematite nanorods. Polymer, 49(18), pp.4000-4008.

[25] Prasanna, B.P., Avadhani, D.N., Raghu, M.S. and Kumar, Y., 2017. Synthesis of polyaniline/α-Fe2O3 nanocomposite electrode material for supercapacitor applications. Materials Today Communications, 12, pp.72-78.

[26] Mirzaei, A., Janghorban, K., Hashemi, B., Hosseini, S.R., Bonyani, M., Leonardi, S.G., Bonavita, A. and Neri, G., 2016. Synthesis and characterization of mesoporous α-Fe2O3 nanoparticles and investigation of electrical properties of fabricated thick films. Processing and Application of Ceramics, 10(4), pp.209-217.

[27] Tang, C. and Liu, W., 2010. Preparation of dual-curable polysiloxane and the properties of its cured films with epoxy resin. Journal of Plastic Film & Sheeting, 26(3), pp.241-257.

[28] Voo, R., Mariatti, M. and Sim, L.C., 2011. Properties of epoxy nanocomposite thin films prepared by spin coating technique. Journal of Plastic Film & Sheeting, 27(4), pp.331-346.

[29] Kanapitsas, A., Tsonos, C., Psarras, G.C. and Kripotou, S., 2016. Barium ferrite/epoxy resin nanocomposite system: Fabrication, dielectric, magnetic and hydration studies. Express Polymer Letters, 10(3), p.227.

[30] Gazderazi, M. and Jamshidi, M., 2016. Hybridizing MWCNT with nano metal oxides and TiO2 in epoxy composites: Influence on mechanical and thermal performances. Journal of Applied Polymer Science, 133(34).

[31] Bhadra, S., Khastgir, D., Singha, N.K. and Lee, J.H., 2009. Progress in preparation, processing and applications of polyaniline. Progress in Polymer Science, 34(8), pp.783-810.

[32] Katsoulis, C., Kandare, E. and Kandola, B.K., 2011. The effect of nanoparticles on structural morphology, thermal and flammability properties of two epoxy resins with different functionalities. Polymer Degradation and Stability, 96(4), pp.529-540.

[33] Wang, Z., Volinsky, A.A. and Gallant, N.D., 2014. Crosslinking effect on polydimethylsiloxane elastic modulus measured by custom-built compression instrument. Journal of Applied Polymer Science, 131(22).

[34] Mohammadzadehmoghadam, S., Dong, Y. and Jeffery Davies, I., 2015. Recent progress in electrospun nanofibers: reinforcement effect and mechanical performance. Journal of Polymer Science Part B: Polymer Physics, 53(17), pp.1171-1212.

[35] Bagheri, S., Chandrappa, K. and Hamid, S.B.A., 2013. Generation of hematite nanoparticles via sol-gel method. Research Journal of Chemical Sciences, 3(7), pp.62-68.

[36] He, C., Sasaki, T., Shimizu, Y. and Koshizaki, N., 2008. Synthesis of ZnO nanoparticles using nanosecond pulsed laser ablation in aqueous media and their self-assembly towards spindle-like ZnO aggregates. Applied Surface Science, 254(7), pp.2196-2202.

[37] Chicot, D., Mendoza, J., Zaoui, A., Louis, G., Lepingle, V., Roudet, F. and Lesage, J., 2011. Mechanical properties of magnetite (Fe3O4), hematite (α-Fe2O3) and goethite (α-FeO· OH) by instrumented indentation and molecular dynamics analysis. Materials Chemistry and Physics, 129(3), pp.862-870.

[38] Siva Sankari, S., Murugan, N., Sivaraj, S., 2014. Effect of Filler Materials on the Mechanical and Thermal Properties of Epoxy Resin. AMM 592–594, 206–210.

[39] Guo, L., Shen, X., Meng, X. and Feng, Y., 2010. Effect of Sm3+ ions doping on structure and magnetic properties of nanocrystalline NiFe2O4 fibers. Journal of Alloys and Compounds, 490(1-2), pp.301-306.

[40] Wang, Z., Liu, X., Lv, M., Chai, P., Liu, Y. and Meng, J., 2008. Preparation of ferrite MFe2O4 (M= Co, Ni) ribbons with nanoporous structure and their magnetic properties. The Journal of Physical Chemistry B, 112(36), pp.11292-11297.

[41] Sivakumar, P., Ramesh, R., Ramanand, A., Ponnusamy, S. and Muthamizhchelvan, C., 2011. Synthesis and characterization of NiFe2O4 nanosheet via polymer assisted co-precipitation method. Materials Letters, 65(3), pp.483-485.

[42] Zhang, C.Y., Shen, X.Q., Zhou, J.X., Jing, M.X. and Cao, K., 2007. Preparation of spinel ferrite NiFe2O4 fibres by organic gel-thermal decomposition process. Journal of Sol-gel Science and Technology, 42(1), pp.95-100.

[43] Rand, B.P., Peumans, P. and Forrest, S.R., 2004. Long-range absorption enhancement in organic tandem thin-film solar cells containing silver nanoclusters. Journal of Applied Physics, 96(12), pp.7519-7526.

[44] Schaadt, D.M., Feng, B. and Yu, E.T., 2005. Enhanced semiconductor optical absorption via surface plasmon excitation in metal nanoparticles. Applied Physics Letters, 86(6), p.063106.

[45] Morfa, A.J., Rowlen, K.L., Reilly III, T.H., Romero, M.J. and van de Lagemaat, J., 2008. Plasmon-enhanced solar energy conversion in organic bulk heterojunction photovoltaics. Applied Physics Letters, 92(1), p.013504.

[46] Jestl, M., Maran, I., Köck, A., Beinstingl, W. and Gornik, E., 1989. Polarization-sensitive surface plasmon Schottky detectors. Optics letters, 14(14), pp.719-721.

[47] Ogwu, A.A., Darma, T.H. and Bouquerel, E., 2007. Electrical resistivity of copper oxide thin films prepared by reactive magnetron sputtering. Journal of Achievements in Materials and Manufacturing Engineering, 24(1), pp.172-177.

[48] Praveena, S.D., Ravindrachary, V. and Bhajantri, R.F., 2016. Dopant-induced microstructural, optical, and electrical properties of TiO2/PVA composite. Polymer Composites, 37(4), pp.987-997.

[49] Khairy, M., 2014. Synthesis, characterization, magnetic and electrical properties of polyaniline/NiFe2O4 nanocomposite. Synthetic metals, 189, pp.34-41.